www.MaterialsViews.com

Boron Nitride

Evolution of Irradiation-Induced Vacancy Defects in Boron Nitride Nanotubes

*Guangming Cheng, Shanshan Yao, Xiahan Sang, Boyi Hao, Dongyan Zhang, Yoke Khin Yap, and Yong Zhu**

Irradiation-induced vacancy defects in multiwalled (MW) boron nitride nanotubes (BNNTs) are investigated via in situ high-resolution transmission electron microscope operated at 80 kV, with a homogeneous distribution of electron beam intensity. During the irradiation triangle-shaped vacancy defects are gradually generated in MW BNNTs under a mediate electron current density (30 A cm^{-2}), by knocking the B atoms out. The vacancy defects grow along a well-defined direction within a wall at the early stage as a result of the curvature induced lattice strain, and then develop wall by wall. The orientation or the growth direction of the vacancy defects can be used to identify the chirality of an individual wall. With increasing electron current density, the shape of the irradiation-induced vacancy defects changes from regular triangle to irregular polygon.

1. Introduction

Hexagonal boron nitride (h-BN), known as "white graphene," has attracted broad interests due to its superb thermal and chemical stabilities, outstanding mechanical properties and high resistance to oxidation.[1–9] Boron nitride nanotube (BNNT) is considered as a structural analogue of carbon nanotube (CNT) by alternating B and N atoms to substitute for C atoms.[3,10] Contrary to CNT, BNNT is a wide band gap (4.5–6.0 eV[11–14]) semiconductor due to the ionic bonding between the atoms. Its electronic properties can be tuned by making hybrid C-BN nanotubes,[15,16] doping or filling with other materials such as metals,[17–19] or introducing bending deformation.[20] Due to the outstanding thermal, mechanical, and physical properties, BNNTs and their composites have promising potentials for applications at high-temperature, hazardous, and high-dose irradiation environments.[21]

Irradiation response of nanomaterials is an interesting topic since the irradiation-induced defects can have an important influence on the microstructure and material properties.[22–30] Irradiation effects on nanomaterials depend on the irradiation source (electron, ion, etc.), dose and microstructures of the materials. Electron beam (e-beam) irradiation on multiwalled (MW) CNTs at room temperature resulted in formation of vacancies on the walls and eventual amorphization under high-dose irradiation.[28,31–33] It was suggested that the atoms sputtered from inner shells remained in the nanotubes and Frenkel pairs created inside the nanotubes can easily recombine.[32,34]

Study on e-beam irradiation of BNNTs, on the other hand, has been scarce. Neighboring BN divacancies and extended defect lines were observed in single-walled (SW) BNNTs with an electron energy of 200 keV.[35] Clustering of multiple vacancies led to extended defects which locally changed the nanotube diameter and chirality. High-dose irradiation on MW BNNTs resulted in gradual amorphization of BN shells followed with complete destruction of the nanotube morphology (electron energy of 300 keV), leaving the material with the consecutive

Dr. G. Cheng, S. Yao, Prof. Y. Zhu
Department of Mechanical and Aerospace Engineering
North Carolina State University
Raleigh, NC 27695, USA
E-mail: yong_zhu@ncsu.edu

Dr. X. Sang, Prof. Y. Zhu
Department of Materials Science and Engineering
North Carolina State University
Raleigh, NC 27695, USA

B. Hao, Dr. D. Zhang, Prof. Y. K. Yap
Department of Physics
Michigan Technological University
Houghton, MI 49931, USA

DOI: 10.1002/smll.201502440

appearance of a near-amorphous BN rod and rectangular onion-like nanoparticle.[8] Moreover, researchers[36] demonstrated "nanomachining" of MW BNNTs (electron energy of 200 keV) to form sharp, crystalline, conical tips and to cut BNNTs for potential applications such as probes for nanomanipulation and imaging.[20] However, the mechanism of irradiation damage of MW BNNTs remains elusive, especially the irradiation-induced vacancy defects, since all the reported results about e-beam irradiation of BNNTs were obtained under high electron energy (200 or 300 keV) that is much higher than the threshold energy to knock out the B and N atoms.

In this study, in situ high-resolution transmission electron microscopy (HRTEM) observation directly revealed the nucleation and development of irradiation-induced vacancy defects, under parallel e-beam (80 keV) with a homogeneous distribution of beam intensity. Triangle-shaped vacancy defects were gradually generated in MW BNNTs by knocking the B atoms out and grew along a well-defined direction within a wall as a result of the curvature induced lattice strain. The effects of the e-beam current density and the number of tube wall on the irradiation damage of MW BNNTs were systematically investigated. With increasing electron current density, the shape of irradiation-induced vacancy defects changed from regular triangle to irregular polygon due to the increasing rate in knocking out B atoms. Finally, the advantage of the e-beam condition used in this work is discussed.

2. Results and Discussion

2.1. Microstructure Characterization

A SW BNNT can be viewed as a single h-BN sheet rolled up into a seamless molecular cylinder, as shown in **Figure 1**a,b. Similar to CNT, BNNT also has the chirality, an important geometrical parameter. The chiral vector (n, m) indicating the rolling direction can be obtained as a linear combination of the basis vectors (shown in the inset in Figure 1b): $n{\cdot}a_1{+}m{\cdot}a_2$. A MW BNNT is typically composed of walls of different chiral types but with a constant interwall (or interplanar) spacing, similar to MW CNT.[37,38]

A TEM image in Figure 1c shows the BNNTs with different diameters and different numbers of tube walls. The distribution of the number of tube walls is shown in Figure 1e, based on 74 nanotubes examined. The number of the tube walls is in the range of 10 to 54 with an average of 28.5. Figure 1d shows an individual MW BNNT with 23 walls as an example. The inset in Figure 1d is the corresponding selected-area electron diffraction (SAED) pattern. The interplanar spacing of the neighboring walls, d_{wall}, was measured as 0.333 nm, which is almost the same as the (0002) planar spacing in h-BN sheet at room temperature.[39] The inner and outer diameters of the nanotubes are labeled as d and D in Figure 1d. Hence, the number of tube walls can be calculated by $N = (D - d)/d_{wall}$. Figure 1f shows the BNNT diameter as a function of the number of tube walls. The inner diameters range from 4.8 to 20.1 nm, while the outer diameters from 12.2 to 50.9 nm. Note that the inner and outer diameters linearly increase with the number of the tube walls when the number is less than 33. But the tube diameters become a bit scattered when the number is more than 33. The difference between the outer and inner diameters is, however, always proportional to the number of the tube walls, confirming the constant interplanar spacing in MW BNNTs.

2.2. Vacancy Nucleation and Growth under E-Beam Irradiation

In situ HRTEM observations revealed the process of irradiation damage and the evolution of irradiation-induced defects

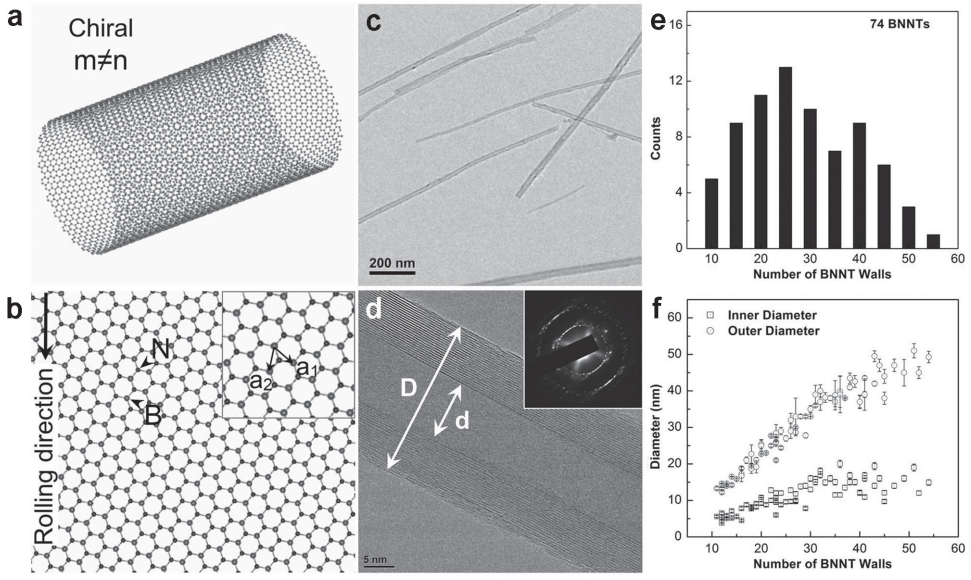

Figure 1. Illustration of a) a SW BNNT rolled from b) the corresponding sheet; Chiral ($m \neq n$). c) Low magnification and d) high-resolution TEM images of MW BNNTs. Insets in (d) is the corresponding SAED pattern. Inner and outer diameters of the nanotubes are labeled as d and D, respectively. e) Distribution of the number of tube walls with the average of 28.5. f) Inner and outer diameters as functions of the number of BNNT walls.

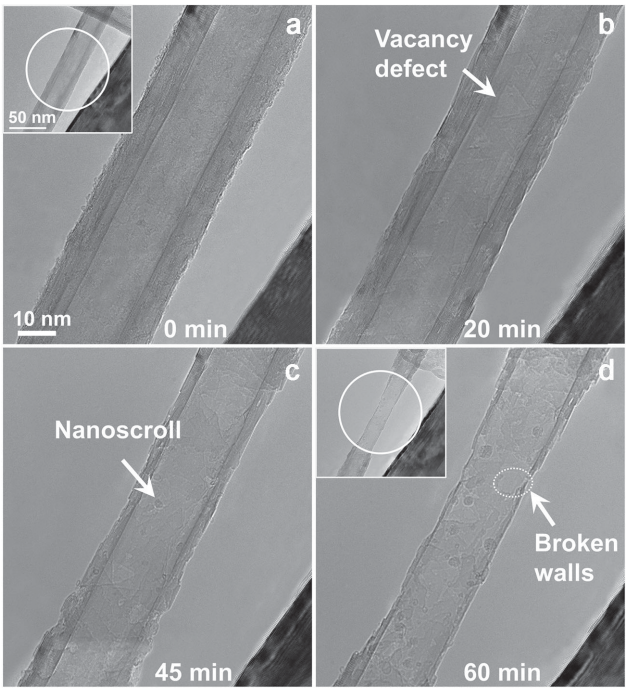

Figure 2. Irradiation damage of an individual MW BNNT (30 walls). The nanotube walls decrease as the time increases. a) 0 min, 30 walls; b) 20 min, 23 walls; c) 45 min, 9 walls; and d) 60 min, 3 walls. Note that to calculate the number of side walls, we took into account the most uniformly damaged part to obtain an average value and set the deviation of the damage walls as error bar in the plots in Figure 5. The insets in (a) and (d) are low magnification images showing the irradiated area marked by the circles (also the beam size). Electron energy, 80 keV; current density, 30 A cm^{-2}.

in an individual MW BNNT with 30 walls under an electron energy of 80 keV and a current density of 30 A cm^{-2} (**Figure 2**). The BNNT side walls were damaged wall by wall until the nanotube was broken; there was no obvious shrinkage and collapse of the outer shells, which was observed previously with an electron energy of 200 keV.[36] This difference is mainly caused by the different distribution of e-beam intensity in the two studies, which will be discussed later in details. Our in situ experiments were conducted under a parallel e-beam with a homogenous distribution of beam intensity. The irradiation damage on the top and bottom walls was almost at the same rate as that on the side walls, regardless of the knock-on directions (see details in Figures S2 and S3, Supporting Information). The irradiation process is described as follows (see Movie S1, Supporting Information). At the initial stage (Figure 2a, 0 min), the nanotube had 30 walls with good atomic structure. The marked circles in the insets of Figure 2a,d correspond to the irradiated area (also the beam size). As the time increased, many irradiation-induced vacancy defects appeared as shown in Figure 2b (20 min). Such vacancy defects have a triangular shape that is similar to the previous results in the thin h-BN sheets and membranes under e-beam irradiation.[40–42] It was suggested that B atoms were knocked out to form such a kind of defects since the operating electron energy (80 keV) was close to the threshold energy (79.5 keV) to knock the B atoms out but far below that (118.6 keV) to knock the N atoms out.[40,43,44] After 45 min (Figure 2c), some "nanoscrolls"[45] appeared on the surface of the nanotube and more came out after 60 min (Figure 2d). Such "nanoscrolls" formed when the dangling part of the damaged walls peeled off during the irradiation. Around 60 min, the breakage of the side and top-bottom walls was observed at the same time, as marked by the dotted ellipse in Figure 2d.

Figure 3 shows the evolution of irradiation-induced vacancy defects for the MW BNNT observed in Figure 2. At the early stage (15–17 min, Figure 3a–c), step-by-step growth of triangle-shaped vacancy defects (marked by I–III) can be clearly seen. Note that each of the triangle-shaped vacancy defects grew along one particular edge, in contrast to the case of thin h-BN membranes where the growth direction could be along any of the three edges.[40] More specifically, a vacancy defect (marked by I in Figure 3a) only developed perpendicular to the edge with an included angle of 60° to the tube axis (Z). Another vacancy defect (marked by II in Figure 3b) appeared at the side of the stable vacancy defect I and grew perpendicular to the other edge with an included angle of 60°to the Z axis. The third vacancy defect (marked by III in Figure 3c) was observed at the corner between defects I and II and grew. It is interesting to note that all three triangle-shaped vacancy defects are oriented in the same way, with one edge parallel to the Z axis and the other two edges with included angles of 60° to the Z axis. As shown in Figure 3d and Figure S5 (Supporting Information), it can be determined that the chiral type of this wall is armchair ($m = n$).

The growth of the three vacancy defects (marked by I–III in Figure 3a–c) at the early stage is illustrated schematically in Figure 3d–i. If only one B atom is knocked out, a single vacancy forms (Figure 3d,e), similar to the case of BN membranes.[40] It was observed that the vacancy defects can grow perpendicular to two edges that have an included angle of 60° to the tube axis (Z) but not perpendicular to the edge parallel to the tube axis. For a vacancy to grow, the B atoms along the edges around the vacancy must be knocked out. To knock out such a B atom, it is plausible that two B—N bonds (nearly) along the edge break followed with the B—N bond perpendicular to the edge (see Figure 3f and Figure S4, Supporting Information). A previous study[35] found that the smaller the nanotube diameter (the larger the curvature), the smaller the formation energy of a vacancy as a result of the curvature-induced lattice strain. In the present case, the two edges that have an included angle of 60° to the tube axis (60° edges) have larger curvature than the edge parallel to the tube axis (parallel edge) (see details in Figure 3d and Figure S3d–f, Supporting Information). The B—N bonds along the 60° edges should be easier to break than those along the parallel edge. Therefore, it is energetically more favorable to knock out the B atoms along the 60° edges. And the vacancy defect grows perpendicular to the two 60° edges since the remaining unstable neighboring N atoms can be sputtered immediately after the knocking out of the B atoms (Figure 3f). Note that for an armchair type SWNT (Figure 3d), the atoms at both the 60° edges should, in theory, have the same possibility of being knocked out at the same time but the knock-out

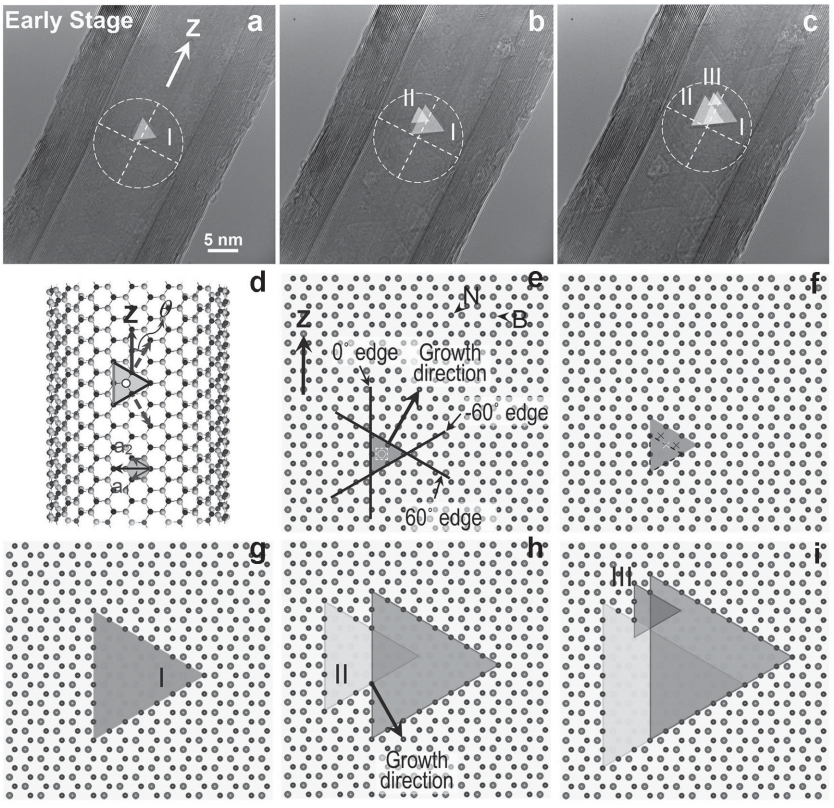

Figure 3. Illustrations of the evolution of irradiation-induced vacancy defects for the MW BNNT observed in Figure 2. a–c) The development of triangle-shaped vacancy defects (marked by I, II, and III) at the early stage (15–17 min). Electron energy, 80 keV; current density, 30 A cm^{-2}. d) A schematic map showing a single vacancy (marked by the triangle) in the single wall with an armchair type (15, 15). The dotted arrows represent the possible growth direction of the single vacancy. The growth direction of the vacancy defect has an included angle (θ) with the tube axis (Z). The dark arrow points out the chiral vector (the rolling direction). e–i) Schematic illustration of atomic models (an armchair type) to describe the nucleation and propagation of irradiation-induced vacancy defects in (a)–(c).

happened only in one direction at a time in our experiment, shown in Figure 3a–c. This might be because the chirality of the tube wall could be slightly different from the armchair type or there might be atomic defects along one particular edge (Figure 3g). Interestingly, the growth of defect II (Figure 3b,h) was along the other 60° edge (different from vacancy defect I). The possible reason is that the B—N bonds at the area close to defect I are weakened by the presence of defect I, which causes that the related B atoms can be easily knocked off. When the 60° edge of defect II encountered the edge of defect I, defect II merged into defect I. Defect III (Figure 3c,i) was not able to grow much since it was constrained by the other two, and instead it quickly merged into defects I and II. After that, the three vacancy defects formed a bigger one that expanded across to the whole surface (see Movie S1, Supporting Information). In short, it can be concluded that the nucleation of vacancy defects follows the following process – a single B atom is first knocked out to form a single vacancy and then the vacancy defect grows step by step in a triangle shape along an energetically favorable direction as a result of the curvature induced lattice strain.

Growth of vacancy defects was further monitored at the advanced stage (44–46 min, **Figure 4**a–c) for the same MW BNNT observed in Figure 2. In this stage the vacancy growth was in a different wall since the outermost wall in Figure 2 was broken. Here a vacancy defect was still in the triangle shape, but none of the three edges of the triangle was along the tube axis direction or radial direction. It suggests that the chirality of this tube wall should be dominated by the chiral type ($m \neq n$), which was different from that at the early stage (armchair type, Figure 3a–c). The growth direction (marked by the arrow in Figure 4a) of the vacancy defect was also perpendicular to the edge with the largest curvature. This further confirmed the selective growth behavior of the triangular vacancy defects in MW BNNTs. Moreover, many small white spots (some of them marked by the arrows in Figure 4b) appeared randomly on the top surface of the outer shells, which were possibly the single vacancies with a diameter of 0.4 nm as compared with the ones in BN sheets.[40] Here the thickness of the nanotube along the incident e-beam direction was reduced by the e-beam and as a result such vacancies can be observed. It appears that under 80 keV irradiation, the damage proceeded wall by wall. It should be emphasized that the orientation or the growth direction of the vacancy defects can provide a simple and useful method to identify the chirality of an individual wall in MW BNNTs by slowly introducing triangle-shaped vacancy defects in it under a relatively low energy (80 keV) e-beam irradiation (see the detailed description in Figure S5, Supporting Information).

2.3. Damage under E-Beam Irradiation

The e-beam irradiation damage is related to the electron energy, electron flux, studied structure and irradiation time. Here the effects of e-beam current density and number of tube walls on the damage processes by in situ HRTEM experiments were further investigated, as shown in **Figure 5**. The

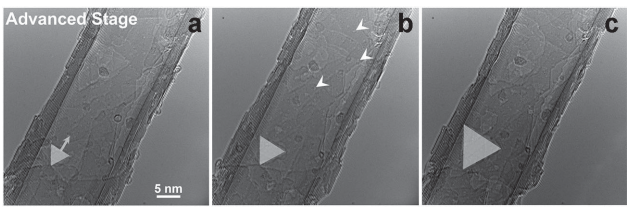

Figure 4. a–c) Growth of an individual triangle-shaped vacancy defect at the advanced stage (44–46 min) for the MW BNNT observed in Figure 2. Electron energy, 80 keV; current density, 30 A cm^{-2}.

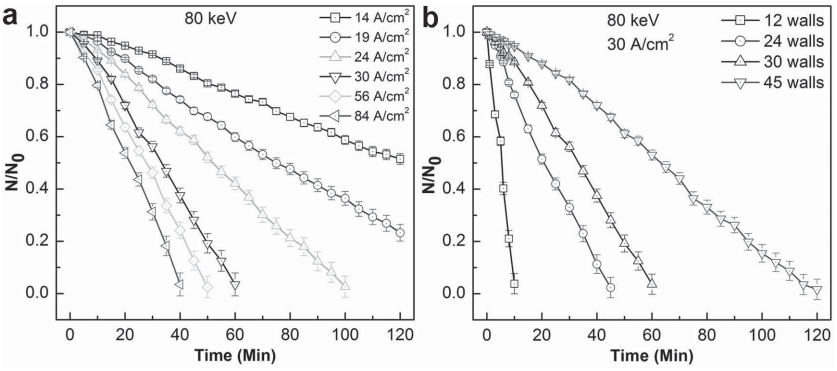

Figure 5. The reduction in the number of BNNT walls as a function of irradiation time. The reduction is normalized to the initial walls of BNNTs. a) Under different current densities but with similar initial numbers of the nanotube walls (28 ± 2). b) BNNTs with different numbers of the nanotube walls under the same current density (30 A cm^{-2}).

electron energy in all experiments was 80 keV. The reduction in the number of the BNNT side walls was plotted as a function of the irradiation time (Figure 5). Note that the reduction in the number of the nanotube walls (N) is normalized to the initial number of walls (N_0) of the MW BNNTs. It can be clearly seen that the reduction is slow at the initial stage and then follows a nearly linear relationship as the time increases, regardless of the current density and the number of the nanotube walls.

As shown in Figure 5a, the reduction rate in the number of the nanotube walls increased with the increasing current density, from 14 to 84 A cm^{-2} (see details in Figure S6, Supporting Information), and the time for the total damage (i.e., breakage of the nanotube) decreased.

The effect of e-beam current density on the microstructure evolution of BNNTs is illustrated in **Figure 6**. Figure 6a–c shows a BNNT under a current density of 56 A cm^{-2}. Both triangle- (marked by I and II) and polygon-shaped (marked by III) vacancy defects were induced in the nanotube. They grew bigger as the irradiation time increased. But for a higher current density (84 A cm^{-2}), only irregular polygon-shaped vacancy defects were observed in Figure 6d–f. The possible reason is that the increase of the irradiation dose (i.e., e-beam current density) will increase the rate of knocking B atoms out and sputtering N atoms out, which cause the quick and random damage of the edges of the vacancy defects. Comparison of the three chosen current densities (30, 56, and 84 A cm^{-2}) clearly shows that the shape of irradiation-induced vacancy defects develops from the regular triangle to the irregular polygon as the e-beam current density increases.

On the other hand, under the same e-beam energy and current density (80 keV and 30 A cm^{-2}), the thin BNNT (12 walls) were much easier to be damaged as compared to the thicker ones (Figure 5b). It took 120 min to totally damage a BNNT with 45 walls, which is 12 times that for a thin one with 12 walls. As the number of tube wall increases, the thickness of the wall increases, which can prolong the damage process (e.g., the time of knocking out atoms). It suggests that increasing the number of tube walls helps to improve the radiation tolerance of BNNTs.

The effect of higher e-beam energy (e.g., 200 keV) on the damage process under the same beam condition was further investigated. The increase of e-beam energy increases the rate of removing B and N atoms. But no shaped vacancy defects can be found in the BNNTs, as shown in **Figure 7**a,b The present study indicates that e-beam with an energy of 80 keV is the favorable condition to observe the shaped vacancy defects and the gradual growth of such defects in MW BNNTs.

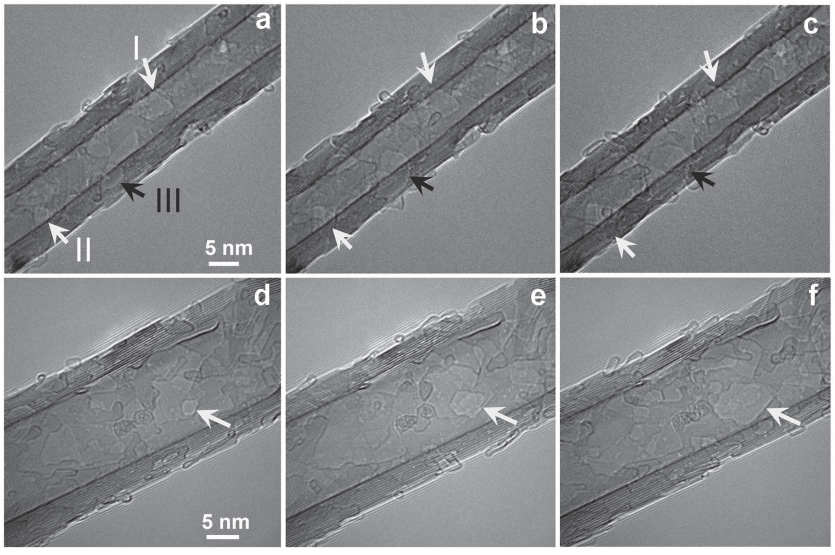

Figure 6. Illustrations of the evolution of irradiation-induced vacancy defects in MW BNNTs as the current density changes. a–c) 56 A cm^{-2}, 10–12 min. d–f) 84 A cm^{-2}, 21–23 min.

2.4. Parallel E-Beam Condition for Irradiation

The e-beam condition in the present study (i.e., parallel e-beam with homogeneous distribution of beam intensity) is important for the investigation of the irradiation-induced vacancy defects in MW BNNTs. Figure 7 shows the effect of the beam conditions on the irradiation damage of MW BNNTs under two different types of TEMs (both at 200 keV and 30 A cm^{-2}) with different distribution of beam intensity (see Figure S7, Supporting Information). Two MW BNNTs with 23 and 25 walls before the irradiation were investigated, as shown in Figure 7a,c, respectively. During the irradiation, no shaped vacancy defect was observed since the e-beam energy (200 keV)

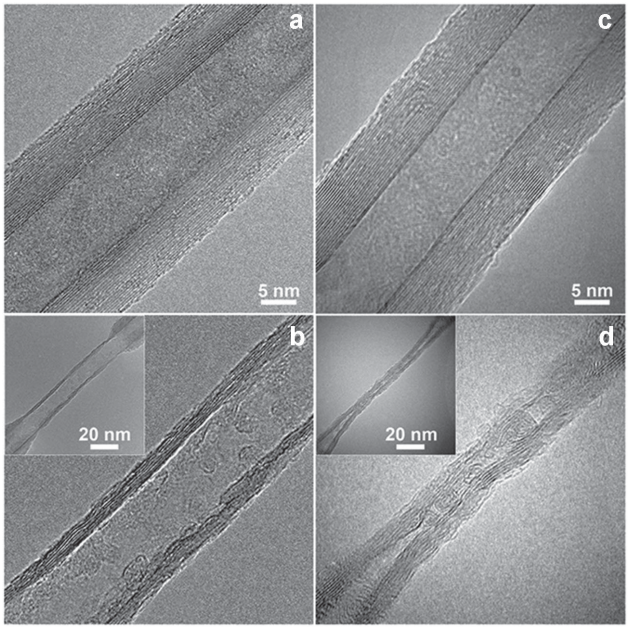

Figure 7. Irradiation damage on MW BNNTs under two types of TEMs, with the same electron energy of 200 keV and current density of 30 A cm^{-2}. a) Before and b) after irradiation from Titan G^2 60–300 (CCD camera, Gatan BM-Ultrascan). c) Before and d) after irradiation from JEOL 2010F (CCD camera, Gatan Orius SC600A2). Insets in (b) and (d) present the corresponding low magnification images showing the seriously irradiated areas.

is much higher than the threshold knock-on energies for B and N. Figure 7b,d shows the snapshots of the two nanotubes after exposing to the e-beam about 30 min. The two nanotubes underwent different damage processes. The one in Figure 7a,b was uniformly damaged, wall by wall, almost from outer to inner; while the other one (Figure 7c,d) was seriously shrunk and collapsed which proceeded through peeling off the layers from both the outer and inner surfaces and bonding of the remaining material. The latter observation is consistent with that reported by Zuo and co-workers,[36] in which the same type of TEM with the same electron energy (e-beam current density, 300 A cm^{-2}) was used.

The difference in the observed phenomena was attributed to the different distribution of e-beam intensity from the two types of TEMs (see Figure S7, Supporting Information). The beam intensity from Titan G^2 60–300 is distributed homogeneously on the CCD camera (used for the nanotube shown in Figure 7a,b), while that from JEOL 2010F has a Gaussian distribution (used for the nanotube shown in Figure 7c,d). Thus, a uniform atom loss from the outer surfaces is proposed for the nanotube uniformly damaged under a parallel e-beam with homogenous distribution of beam intensity. In contrast, anisotropic knock-on (especially the damage of the inner walls) is possible for causing the nanotube shrinkage and collapse under a concentrated e-beam, which is consistent with the work of Smith and Luzzi.[46]

In short, the homogeneous distribution of beam intensity mainly contributed to the observation of irradiation induced vacancy defects and uniform wall damage in MW BNNTs, while the concentrated beam intensity resulted in the serious shrunk and collapsed phenomena. It is worth noting that the e-beam condition with homogenous distribution of beam intensity well imitates the real irradiation environment with spreading particles from nuclear power reaction, outerspace, etc.

3. Conclusions

Irradiation-induced vacancy defects in MW BNNTs were systematically investigated under parallel e-beam (80 keV) with a homogeneous distribution of beam intensity, including the effects of e-beam current density and nanotube wall on the irradiation damage. Under a mediate e-beam current density (30 A cm^{-2}), vacancy defects with triangular shape were induced in MW BNNTs by knocking the B atoms out. The vacancy defects grew along a well-defined direction within a wall at the early stage as a result of the curvature induced lattice strain and developed wall by wall during the irradiation. Such triangular vacancy defects were aligned on an individual wall, which can be used to deduce the chirality of the wall. As the increase of electron current density, the shape of irradiation-induced vacancy defects developed from regular triangle to irregular polygon due to the increased rate of knocking out B atoms. The irradiation damage on MW BNNTs was going through wall by wall, from outer to inner. Increasing the number of tube walls was helpful to improve the radiation tolerance of BNNTs. The e-beam condition with a homogeneous distribution of beam intensity can imitate the real irradiation environment with spreading particles from nuclear power reaction, outerspace, etc. The insights into the defect nucleation and evolution of BNNTs under e-beam irradiation learned from this work could be applied to other types of nanotubes and 2D layered materials (e.g., BN membranes).

4. Experimental Section

Sample Preparation: The MW BNNTs studied here were grown by thermal chemical vapor deposition (CVD) at 1100–1200 °C.[47] The samples for in situ HRTEM experiments were prepared by depositing BNNTs from a dispersion of nanotubes in ethanol onto the copper grids covered with lacey carbon film (no Formvar).

Characterization: High energy electron irradiation study was carried out with a probe corrected (monochromator) FEI Titan G^2 60–300 kV scanning transmission electron microscope (S/TEM) equipped with an extreme field emission gun (X-FEG) source operating at 80 and 200 keV, and a JEOL 2010F transmission electron microscope (TEM) with a Schottky field emission gun (FEG) operating at 200 keV. E-beam current densities used in the experiments were obtained by calculating the counts on the CCD camera for FEI Titan G^2 60–300 kV S/TEM and evaluating the values from the previous report[48] for JEOL 2010F.

Supporting Information

Supporting Information is available from the Wiley Online Library or from the author.

Acknowledgements

This project was supported by the US Department of Energy Nuclear Energy University Program (NEUP) under award 11–3225 and in part by the National Science Foundation (NSF) under award CMMI-1301193. The authors acknowledge the use of the Analytical Instrumentation Facility (AIF) at North Carolina State University, which is supported by the State of North Carolina and NSF. Y.K.Y. acknowledges the support from the National Science Foundation, Division of Materials Research (Award No. 1261910). These acknowledgements were updated on February 10, 2016.

[1] D. Golberg, Y. Bando, C. C. Tang, C. Y. Zhi, *Adv. Mater.* **2007**, *19*, 2413.
[2] D. Golberg, Y. Bando, Y. Huang, T. Terao, M. Mitome, C. Tang, C. Zhi, *ACS Nano* **2010**, *4*, 2979.
[3] R. Arenal, X. Blase, A. Loiseau, *Adv. Phys.* **2010**, *59*, 101.
[4] H. Zeng, C. Zhi, Z. Zhang, X. Wei, X. Wang, W. Guo, Y. Bando, D. Golberg, *Nano Lett.* **2010**, *10*, 5049.
[5] J. Wang, C. H. Lee, Y. K. Yap, *Nanoscale* **2010**, *2*, 2028.
[6] L. Ci, L. Song, C. Jin, D. Jariwala, D. Wu, Y. Li, A. Srivastava, Z. F. Wang, K. Storr, L. Balicas, F. Liu, P. M. Ajayan, *Nat. Mater.* **2010**, *9*, 430.
[7] N. G. Chopra, R. J. Luyken, K. Cherrey, V. H. Crespi, M. L. Cohen, S. G. Louie, A. Zettl, *Science* **1995**, *269*, 966.
[8] D. Golberg, Y. Bando, W. Han, L. Bourgeois, K. Kurashima, T. Sato, *MRS Online Proc. Library* **1999**, *593*, 27.
[9] Y. Lin, J. W. Connell, *Nanoscale* **2012**, *4*, 6908.
[10] O. L. Krivanek, M. F. Chisholm, V. Nicolosi, T. J. Pennycook, G. J. Corbin, N. Dellby, M. F. Murfitt, C. S. Own, Z. S. Szilagyi, M. P. Oxley, S. T. Pantelides, S. J. Pennycook, *Nature* **2010**, *464*, 571.
[11] R. Arenal, O. Stéphan, M. Kociak, D. Taverna, A. Loiseau, C. Colliex, *Phys. Rev. Lett.* **2005**, *95*, 127601.
[12] J. Wang, V. K. Kayastha, Y. K. Yap, Z. Fan, J. G. Lu, Z. Pan, I. N. Ivanov, A. A. Puretzky, D. B. Geohegan, *Nano Lett.* **2005**, *5*, 2528.
[13] R. Czerw, S. Webster, D. L. Carroll, S. M. C. Vieira, P. R. Birkett, C. A. Rego, S. Roth, *Appl. Phys. Lett.* **2003**, *83*, 1617.
[14] C. H. Lee, M. Xie, V. Kayastha, J. Wang, Y. K. Yap, *Chem. Mater.* **2010**, *22*, 1782.
[15] D. Golberg, Y. Bando, P. Dorozhkin, Z.-C. Dong, *MRS Bull.* **2004**, *29*, 38.
[16] W.-Q. Han, J. Cumings, X. Huang, K. Bradley, A. Zettl, *Chem. Phys. Lett.* **2001**, *346*, 368.
[17] H. Chen, Y. Chen, C. P. Li, H. Zhang, J. S. Williams, Y. Liu, Z. Liu, S. P. Ringer, *Adv. Mater.* **2007**, *19*, 1845.
[18] H. J. Xiang, J. Yang, J. G. Hou, Q. Zhu, *New J. Phys.* **2005**, *7*, 39.
[19] D. Golberg, F. F. Xu, Y. Bando, *Appl. Phys. A* **2003**, *76*, 479.
[20] H. M. Ghassemi, C. H. Lee, Y. K. Yap, R. S. Yassar, *Nanotechnology* **2012**, *23*, 105702.
[21] BNNT Proposed applications, http://www.bnnt.com/resources/applications (accessed: July **2015**).
[22] A. Kis, G. Csanyi, J. P. Salvetat, T.-N. Lee, E. Couteau, A. J. Kulik, W. Benoit, J. Brugger, L. Forro, *Nat. Mater.* **2004**, *3*, 153.
[23] A. V. Krasheninnikov, F. Banhart, *Nat. Mater.* **2007**, *6*, 723.
[24] B. Peng, M. Locascio, P. Zapol, S. Li, S. L. Mielke, G. C. Schatz, H. D. Espinosa, *Nat. Nano* **2008**, *3*, 626.
[25] O. Lehtinen, T. Nikitin, A. V. Krasheninnikov, L. Sun, F. Banhart, L. Khriachtchev, J. Keinonen, *New J. Phys.* **2011**, *13*, 073004.
[26] M. Radosavljević, J. Appenzeller, V. Derycke, R. Martel, P. Avouris, A. Loiseau, J.-L. Cochon, D. Pigache, *Appl. Phys. Lett.* **2003**, *82*, 4131.
[27] J. Cumings, A. Zettl, *Solid State Commun.* **2004**, *129*, 661.
[28] C. Mikó, M. Milas, J. W. Seo, E. Couteau, N. Barišić, R. Gaál, L. Forró, *Appl. Phys. Lett.* **2003**, *83*, 4622.
[29] M. Locascio, B. Peng, P. Zapol, Y. Zhu, S. Li, T. Belytschko, H. D. Espinosa, *Exp. Mech.* **2009**, *49*, 169.
[30] Y. Wang, H. J. Joyce, Q. Gao, X. Liao, H. H. Tan, J. Zou, S. P. Ringer, Z. Shan, C. Jagadish, *Nano Lett.* **2011**, *11*, 1546.
[31] F. Banhart, *Rep. Prog. Phys.* **1999**, *62*, 1181.
[32] A. V. Krasheninnikov, K. Nordlund, *J. Appl. Phys.* **2010**, *107*, 071301.
[33] F. Banhart, J. Li, M. Terrones, *Small* **2005**, *1*, 953.
[34] J. P. Salvetat, J. M. Bonard, N. H. Thomson, A. J. Kulik, L. Forró, W. Benoit, L. Zuppiroli, *Appl. Phys. A* **1999**, *69*, 255.
[35] A. Zobelli, C. P. Ewels, A. Gloter, G. Seifert, O. Stephan, S. Csillag, C. Colliex, *Nano Lett.* **2006**, *6*, 1955.
[36] A. Celik-Aktas, J. F. Stubbins, J.-M. Zuo, *J. Appl. Phys.* **2007**, *102*, 024310.
[37] C. Zhi, Y. Bando, C. Tang, D. Golberg, *Mater. Sci. Eng.: R: Rep.* **2010**, *70*, 92.
[38] L.-C. Qin, *Phys. Chem. Chem.l Phys.* **2007**, *9*, 31.
[39] W. Paszkowicz, J. B. Pelka, M. Knapp, T. Szyszko, S. Podsiadlo, *Appl. Phys. A* **2002**, *75*, 431.
[40] J. C. Meyer, A. Chuvilin, G. Algara-Siller, J. Biskupek, U. Kaiser, *Nano Lett.* **2009**, *9*, 2683.
[41] C. Jin, F. Lin, K. Suenaga, S. Iijima, *Phys. Rev. Lett.* **2009**, *102*, 195505.
[42] S. Okada, *Phys. Rev. B* **2009**, *80*, 161404.
[43] J. Kotakoski, C. H. Jin, O. Lehtinen, K. Suenaga, A. V. Krasheninnikov, *Phys. Rev. B* **2010**, *82*, 113404.
[44] A. Zobelli, A. Gloter, C. P. Ewels, G. Seifert, C. Colliex, *Phys. Rev. B* **2007**, *75*, 245402.
[45] J. S. Kim, K. B. Borisenko, V. Nicolosi, A. I. Kirkland, *ACS Nano* **2011**, *5*, 3977.
[46] B. W. Smith, D. E. Luzzi, *J. Appl. Phys.* **2001**, *90*, 3509.
[47] C. H. Lee, J. Wang, V. K. Kayatsha, J. Y. Huang, Y. K. Yap, *Nanotechnology* **2008**, *19*, 455605.
[48] W. Xu, Y. Zhang, G. Cheng, W. Jian, P. C. Millett, C. C. Koch, S. N. Mathaudhu, Y. Zhu, *Nat. Commun.* **2013**, *4*, 2288.

Received: August 13, 2015
Revised: October 23, 2015
Published online: December 18, 2015